

Structural Characterization of the Cooperativity of Unfolding of a Heterodimeric Protein using Hydrogen Exchange-Mass Spectrometry

Rupam Bhattacharjee and Jayant B. Udgaonkar*

National Centre for Biological Sciences, Tata Institute of Fundamental Research, Bangalore, India
Indian Institute of Science Education and Research, Pune, India

Correspondence to Jayant B. Udgaonkar: Indian Institute of Science Education and Research, Pune, India
jayant@iiserpune.ac.in (J.B. Udgaonkar); [@Rupam_B01](https://twitter.com/Rupam_B01) (R. Bhattacharjee)
<https://doi.org/10.1016/j.jmb.2021.167268>

Edited by Sheena E. Radford

Abstract

Little is known about how the sequence of structural changes in one chain of a heterodimeric protein is coupled to those in the other chain during protein folding and unfolding reactions, and whether individual secondary structural changes in the two chains occur in one or many coordinated steps. Here, the unfolding mechanism of a small heterodimeric protein, double chain monellin, has been characterized using hydrogen exchange-mass spectrometry. Transient structure opening, which enables HX, was found to be describable by a five state $N \leftrightarrow I_1 \leftrightarrow I_2 \leftrightarrow I_3 \leftrightarrow U$ mechanism. Structural changes occur gradually in the first three steps, and cooperatively in the last step. β strands 2, 4 and 5, as well as the α -helix undergo transient unfolding during all three non-cooperative steps, while $\beta 1$ and the two loops on both sides of the helix undergo transient unfolding during the first two steps. In the absence of GdnHCl, only $\beta 3$ in chain A of the protein unfolds during the last cooperative step, while in the presence of 1 M GdnHCl, not only $\beta 3$, but also $\beta 2$ in chain B unfolds cooperatively. Hence, the extent of cooperative structural change and size of the cooperative unfolding unit increase when the protein is destabilized by denaturant. The naturally evolved two-chain variant of monellin folds and unfolds in a more cooperative manner than does a single chain variant created artificially, suggesting that increasing folding cooperativity, even at the cost of decreasing stability, may be a driving force in the evolution of proteins.

© 2021 Elsevier Ltd. All rights reserved.

Introduction

The folding reactions of many small proteins have usually been studied by ensemble averaging probes such as fluorescence and circular dichroism, and found to be describable by a two-state transition between the unfolded (U) and native (N) states. These studies have led to the belief that naturally occurring proteins have evolved to fold in a two-state manner^{1–3} without populating partially folded intermediate structures that could potentially aggregate.⁴ Nevertheless, the two-state description does not preclude the transient population of high energy intermediates. Indeed such intermediates have

been detected, when looked for, by hydrogen exchange (HX)^{5–10} as well as by sulfhydryl labelling (SX)^{11,12} experiments, and their characterization has enabled delineation of the sequence of structural change. Moreover, the folding reactions of many proteins have been shown to proceed *via* the transient population of folding intermediates that are stable enough to accumulate sufficiently to be detected.^{13–17} The limited cooperativity inherent in the folding reactions of many proteins has made possible detailed structural characterization of their folding pathways.

When methods such as time-resolved fluorescence resonance energy transfer (tr-FRET),^{18–20}

single-molecule FRET²¹ or hydrogen exchange-mass spectrometry (HX-MS),^{10,22,23} are used to study folding or unfolding reactions, not only can they reveal the sequence of structural changes, but they can also identify and quantify the populations of co-existing conformations. These methodologies have enabled extreme non-cooperativity to be observed, which manifests itself as gradual continuous transitions between conformations populated during folding.^{24–28} Clearly, folding need not be slowed down by only a single or a few dominant (5–10 $k_B T$) barriers, but may be slowed down by a large number of distributed small (1–3 $k_B T$) barriers.^{29–31}

Both tr-FRET^{28,32} and HX-MS¹⁰ measurements have proven to be of great utility in revealing the sequence of structural events, and in bringing out the lack of cooperativity in the folding reactions of the small protein monellin in its artificially created single chain variant, MNEI. MNEI is a single chain variant of the naturally occurring, double chain monellin (dcMN), in which the C-terminus of chain B is covalently connected *via* a Gly-Phe linker, to the N-terminus of chain A (Figure 1). The structures of MNEI and dcMN are virtually identical^{33,34} except at the linker region (Figure 1). Kinetic studies utilizing the tr-FRET method have revealed continuous loss of structure during unfolding.²⁸ It has also revealed which segments of structure undergo continuous change.³⁵ The tr-FRET studies have also revealed how multiple folding pathways of MNEI differ in the sequence of structure forming events.^{36,37} The HX-MS method has revealed that the unfolding and refolding reactions are gradual in strongly refolding conditions in the absence of denaturant, and gain limited cooperativity in the presence of denaturant. It has revealed, as has the tr-FRET method, that the sole helix forms gradually during folding.³⁸ The HX-MS method has brought out elegantly how the cooperativity of a folding reaction is related intimately to protein stability.^{10,39–41}

Surprisingly, dcMN appears to be more stable than MNEI when the usual standard state protein

concentration of 1 M is used to calculate the stabilities of the proteins. The standard free energy of unfolding, ΔG^0 , was found to be 6.3 kcal.mol⁻¹ and 11.4 kcal.mol⁻¹ at pH 8 for MNEI and dcMN, respectively.^{12,34} It is not known how the pathways of folding and unfolding of dcMN differ in structural terms from those of the less stable MNEI. Nor is it known how the greater apparent stability of dcMN affects the cooperativity of its folding-unfolding reactions, and whether the lack of cooperativity observed for MNEI is due to the artificial linking together, covalently, of the two chains of naturally evolved dcMN.

Here, HX-MS studies of dcMN have been carried out to determine the sequence of structural events during transient unfolding in native conditions. An important goal was to resolve whether the (un)folding reactions of the naturally occurring dcMN lack cooperativity to the same extent as that of the artificially created single chain variant, MNEI. The study was also carried out to test the relationship between cooperativity and stability, revealed by previous studies on MNEI. It is shown that the unfolding of dcMN occurs *via* three continuous non-cooperative phases of structure loss are followed by a final cooperative phase. All the phases of exchange/unfolding show strong dependences on denaturant concentration, suggesting that the partially unfolded intermediates formed transiently at the end of each kinetic phase are high free energy intermediates. High resolution segment-specific structural analysis reveals that only the $\beta 3$ strand of chain A of dcMN undergoes cooperative unfolding in the absence of denaturant, while all other secondary structural units complete their transient unfolding during the three non-cooperative phases. The cooperativity of unfolding increases in the presence of 0.6–1 M GdnHCl: the $\beta 2$ strand of chain B as well opens up cooperatively along with the $\beta 3$ strand of chain A.

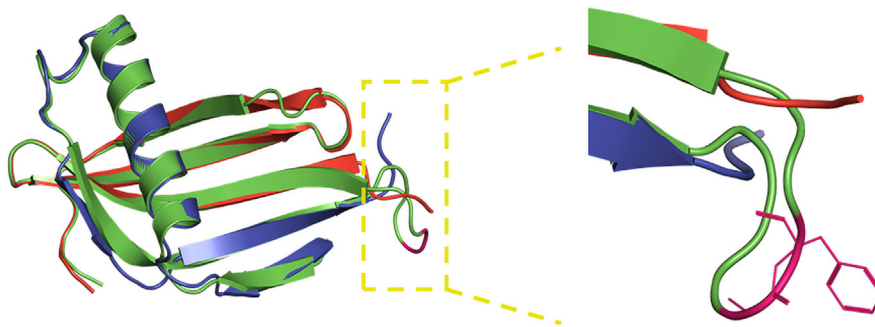


Figure 1. Structural comparison of MNEI and dcMN. Panel a shows the structural alignment of main chain peptide backbones of MNEI (in green) and dcMN (in blue and red). Chain B of dcMN is shown in blue, while chain A is shown in red. The Gly-Phe linker which is shown in pink, joins the two chains of dcMN to yield MNEI. The structures were drawn using the Pymol software and the PDB ID 11V7 and 3MON.

Results

HX kinetics in the absence of denaturant

To determine the kinetics of HX into the individual chains B and A, mass distributions corresponding to the +7 charge state (the most intense one) were obtained at different times of exchange. The back-exchange control showed that 49 ± 1 deuteriums were retained by these two chains together. At 5 s of HX, 33 ± 1 deuteriums were retained, indicating that 16 ± 1 deuteriums were weakly protected and exchanged out rapidly. The remaining 33 ± 1 deuteriums, out of which 16 ± 1 were in chain B and 17 ± 1 were in chain A, served as probes for structure.

The mass distribution of chain B shifted gradually to lower mass with time in three non-cooperative kinetic phases, remaining unimodal over the entire time of HX (Figures 2(a) and (b)). On the other hand, the mass distribution of chain A was found to remain unimodal and shift gradually to lower mass with time in three non-cooperative kinetic phases, over an initial period of exchange time (Figure 2(c)), but showed bimodality later during exchange (Figure 2(d)) when exchange occurred in a cooperative kinetic phase. Figure 2(e) and (f) show three well-separated non-cooperative kinetic phases of exchange for chain B and chain A,

respectively. The peak width (FWHM) of the chain B mass distributions showed a small but consistent decrease with time of HX. The difference in peak width between the first and last timepoints was 2.8 Da which could be explained by accounting for a decrease in stochastic isotopic heterogeneity due to fewer deuteriums being retained at longer times than at initial times of HX (Figure 2(g)).⁴²

The appearance of the low m/z peak at later time points for chain A corresponded to the appearance of completely exchanged chain A. The fractional area under this peak increased exponentially with time (Figure 2(h)). This slowest phase of exchange corresponded to transient sampling of the globally unfolded state. The mass difference between the two well-separated peaks in the bimodal mass distribution was 7 ± 1 Da, indicating that 7 ± 1 amide sites opened up cooperatively to transiently sample the globally unfolded state. In the case of chain B, the rate constant of transient global unfolding could not be determined in a similar manner, as its mass distribution remained unimodal over the entire range of exchange times. This indicated that all amide deuteriums had exchanged out from chain B, before the slowest cooperative phase of HX occurred in dcMN.

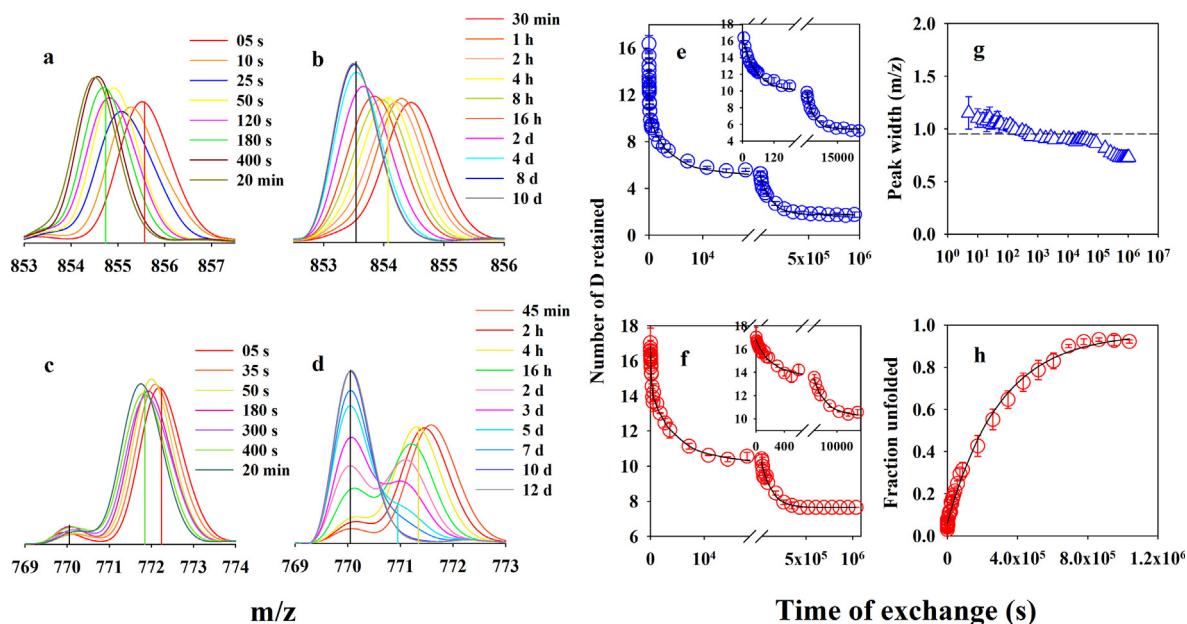


Figure 2. Hydrogen exchange kinetics of dcMN in the absence of GdnHCl at pH 8, 25 °C. Representative mass spectra (+7 charge state for both the chains) are shown for the exchange of chain B (panels a, b) and chain A (panels c, d). The vertical solid lines represent the centroid m/z values for the N state (5 s, red line), U state (10 d, gray line) and for the intermediate species formed at the end of each kinetic phase of exchange. The plots of the number of deuteriums retained as a function of time of exchange for chain B (panel e) and chain A (panel f) are fit to the sum of three exponential equations. The insets show the fast and slow phases of exchange. Panel g shows the dependence of the peak width (full width at half maximum) of the mass distributions on time of exchange for chain B. The broken line was drawn by inspection to guide the eye. Panel h shows that the increase in the fraction of completely exchanged chain A, with time of exchange, fits well to a single exponential equation with a rate constant of $(3.4 \pm 0.3) \times 10^{-6} \text{ s}^{-1}$. The error bars show the standard deviations in the data obtained from two separate experiments.

HX occurred in the EX1 regime

Correct interpretation of HX kinetics data required accurate determination of whether HX occurred in the EX1 or EX2 or EXX regime.^{6,10,43–46} The bimodal mass distributions observed during the cooperative phase of HX for chain A suggested that HX had occurred in the EX1 regime.^{10,40,46,47} The gradual shift in the unimodal mass distributions seen in Figure 2 suggested, however, the possibility that HX might have occurred in the EX2 and not in the EX1 regime, through very localized structural openings.

To distinguish between the EX1 and EX2 regimes, it was necessary to examine the pH dependence of the observed rate constants of HX.⁴⁵ The observed rate constant of exchange in the EX2 regime is expected to increase 10-fold with a unit increase in pH, and to be independent of pH in the EX1 regime. When the HX reaction was carried out at pH 7, 8 and 9, the rate constants of each kinetic phase, for both the chains, were found to be independent of pH (Figure S1). Thus, for both the chains, the HX reaction occurred in the EX1 regime in each of the kinetic phases. The observation that the rate constants of the very slow phase of HX into chain B and chain A, and the global unfolding rate constant measured only for chain A, were marginally higher at pH 9 than at pH 7 and pH 8, can possibly be accounted for by the decreased stability of dcMN at higher pH.³⁴

HX kinetics in the presence of denaturant

The equilibrium denaturation midpoint (C_m) of dcMN is 0.7 M GdnHCl at pH 8, 25 °C and 10 μ M protein concentration (Figure S2). In the presence of low concentrations of GdnHCl such as 0.2 and 0.4 M, both chains showed exchange behavior similar to that seen in 0 M GdnHCl. The mass distribution of chain B shifted gradually towards a lower m/z as a unimodal peak throughout the reaction (Figures S3(a), (b), S4(a) and (b)), as it did in the absence of GdnHCl. Similarly, the mass distribution of chain A remained unimodal during the initial phase of exchange shifting gradually from higher to lower m/z (Figures S3(c) and S4(c)), but became bimodal when exchange became cooperative later on (Figures S3(d) and S4(d)). Chain B exchanged all of its deuteriums in three non-cooperative kinetic phases characterized by shifts in a unimodal mass distribution (Figures S3(e) and S4(e)). The width of the mass distributions of chain B decreased by 2 Da with time of HX (Figures S3(f) and S4(f)). The change in peak width, which was due to fewer deuteriums being retained at longer times than initial times of HX, was not very significant. Chain A lost all of its deuteriums in four kinetic phases: the first three were non-cooperative (Figures S3(g) and S4(g)) and the fourth slowest phase was cooperative

(Figures S3(h) and S4(h)). The number of deuteriums that exchanged out cooperatively in the slowest phase of exchange in chain A remained constant across the GdnHCl concentration range of 0 to 0.4 M. Each of these kinetic phases, as expected, become faster in the presence of denaturant. No significant change in the amplitude of each phase was observed across this concentration range of denaturant (0–0.4 M) (Tables 1 and S1).

At denaturant concentrations (0.6–1 M) near the C_m of dcMN, chain B showed a gradual shift in its mass distribution at initial times of HX (Figures 3(a), S5(a) and S6(a)), and a broadening in its mass distribution later on, which could not be fit to a single Gaussian distribution anymore. Instead, the mass distributions fitted better to two Gaussian distributions, indicating more cooperative structural opening (Figures 3(a), S5(b) and S6(b)). The high m/z population lost all of its remaining deuteriums cooperatively, and completely exchanged-out protein appeared as the lower m/z population. Figure S7 shows an increase in the peak width (FWHM) of the isotopic distribution, which also indicated the cooperative unfolding of chain B in the presence of 0.6 to 1 M GdnHCl. On the other hand, chain A exchanged out in a manner similar to how it exchanged out at lower GdnHCl concentrations (Figures 3(b), S5(c), (d), S6(c) and (d)). The dependence of the number of deuteriums retained on the time of exchange fit well to the sum of three exponential equations, for both the chains (Figures 3(c), (d), S5(e), (f), S6(e) and (f)). The fractional area under the low m/z mass distribution increased in an exponential manner with the time of exchange (Figures 3(e), (f), S5(g), (h), S6(g) and (h)). These results suggested that the exchange happened in four kinetic phases in these solvent conditions for both chains B and A: three non-cooperative phases and a slowest cooperative phase. 4 ± 1 deuteriums in chain B, and 7 ± 1 deuteriums in chain A exchanged out cooperatively in the slowest phase of exchange, with similar rate constants (Tables 2 and S1).

Denaturant dependence of exchange and global unfolding rates

Figure 4(a) shows that the rate constants of HX at all GdnHCl concentrations were the same for chains A and B, for the fast, slow and very slow phases of exchange. Consequently, the observed rate constants of HX for both chains had the same dependence on GdnHCl concentration. Figure 4(a) also shows that the slowest cooperative phase had the same rate constants at 0.6–1 M GdnHCl, for both chains. This slowest cooperative phase was not observed for chain B at 0–0.4 M GdnHCl. The rate constants of exchange/unfolding for all of

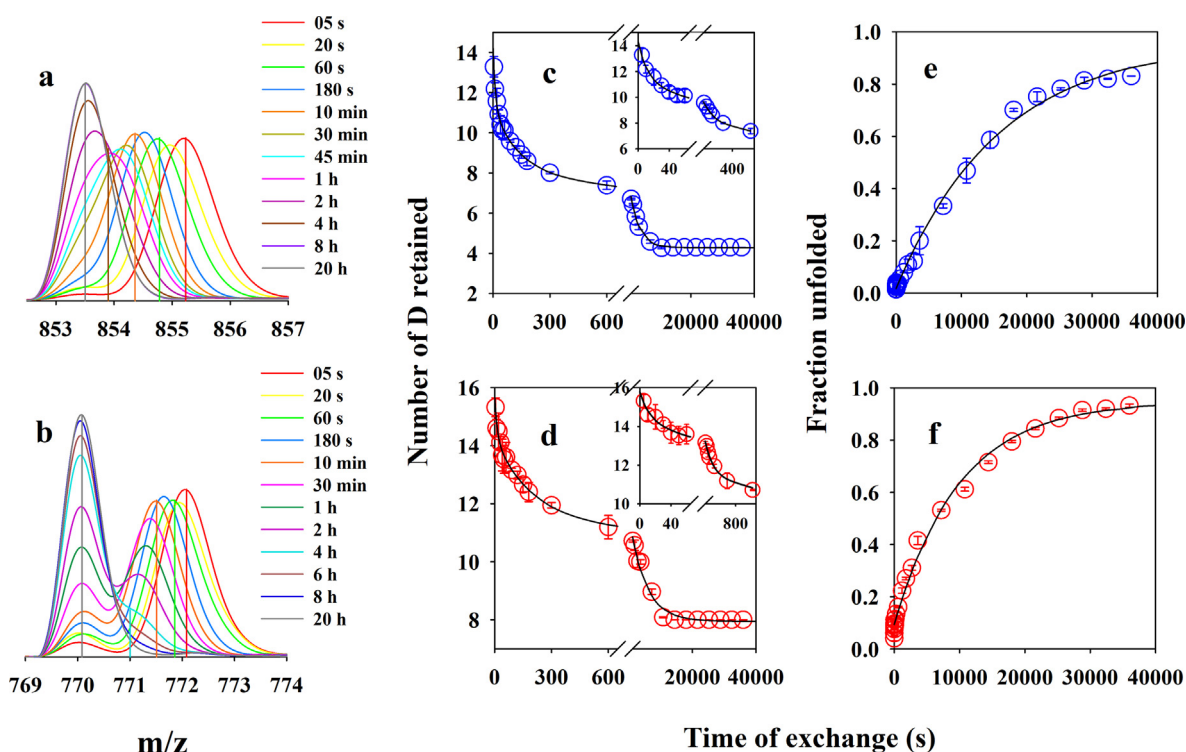


Figure 3. Hydrogen exchange kinetics of dcMN in 1 M GdnHCl at pH 8, 25 °C. Representative mass spectra (+7 charge state for both the chains) are shown for chain B (panel a) and chain A (panel b). The solid vertical lines represent the centroid m/z values of the N state (5 s, red line), U state (20 h, gray line) and the intermediate species formed at the end of each kinetic phase. Panels c and d show the dependences of the number of deuteriums retained on the time of exchange, for chains B and A, respectively. In both cases, the data fit well to the sum of three exponentials. Panels e and f show that the increase in the fraction of completely exchanged protein with time fits to a single exponential equation for both chains B and A, yielding global unfolding rate constants of $(63.5 \pm 10.2) \times 10^{-6} \text{ s}^{-1}$ and $(101 \pm 2.2) \times 10^{-6} \text{ s}^{-1}$ for chain B (panel e) and chain A (panel f), respectively. The error bars show the standard deviations in the data obtained from two independent experiments.

the phases increased with the concentration of GdnHCl, indicating that unfolding exposed more solvent-accessible surface area and that the transition states were stabilized by the denaturant.

The rate constants of global unfolding at higher denaturant concentrations were also determined by measurement of intrinsic Trp fluorescence at pH 7, 8 and 9 (Figure S8). The rate constants of the slowest cooperative phase seen by HX measurement at GdnHCl concentrations greater than 0.6 M, by which both chains A and B transiently populate the globally unfolded state, were predicted by the linear extrapolation of the dependence of the logarithm of the observed rate constants of unfolding on GdnHCl concentration. The HX monitored rate constants of global exchange/unfolding at GdnHCl concentrations lower than 0.4 M, were found to be slower than the extrapolated fluorescence-monitored rate constants of global unfolding, and a downward kink was observed in the dependence of the logarithm of the unfolding rate constant on GdnHCl concentration (Figure 4(b)).

Kinetic simulations of unfolding

The kinetic data indicated that the exchange occurred in an uncorrelated manner in three phases, which were followed by a correlated phase of exchange. The observation that HX occurred in four kinetic phases, well-separated in their timescales, suggested that, minimally, the unfolding mechanism must have four discrete steps in order to be able to account for the data. It appeared that fast opening events in one or more segments of the native structure led to the transient sampling of a partially unfolded intermediate I_1 , that slow opening events led to the transient sampling of a partially unfolded intermediate I_2 , and that very slow opening events led to the transient sampling of a partially unfolded intermediate I_3 . The slowest opening events occurred cooperatively and led to the transient sampling of the completely unfolded state, U. Simulations to different kinetic models incorporating N, I_1 , I_2 , I_3 and U were carried out (see SI) to determine the simplest scheme that could account for the time course of change in the

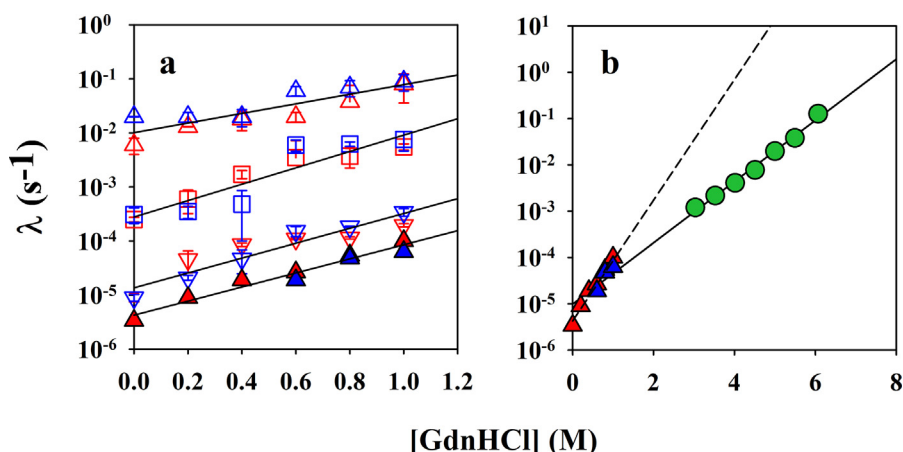


Figure 4. Dependences of the rate constants of the different kinetic phases of HX at pH 8, and of intrinsic Trp fluorescence-monitored global unfolding, on denaturant concentration. In both cases, data were collected at 10 μ M protein concentration. The red and blue symbols denote the observed rate constants for chains A and B, respectively. (a) Open symbols represent the rate constants of exchange measured from the shift in the centroid m/z of the mass distributions with time. Δ , \triangle , the rate constants of the fast phase of HX; \square , \square , the rate constants of the slow phase of HX; ∇ , ∇ , the rate constants of the very slow phase of HX; \blacktriangle , \blacktriangle , the observed rate constants of transient formation of the globally unfolded state determined by measuring the increase in the area of the fully exchanged out peak with time. The solid lines are the linear fits to the dependences of the logarithm of the rate constants of each phase for both the chains, and have slopes of 0.9 M⁻¹ (fast phase), 1.5 M⁻¹ (slow phase) and 1.4 M⁻¹ (very slow phase). (b) Global unfolding rate constants monitored by measurement of the change in intrinsic Trp fluorescence at 340 nm (green filled circles). Red and blue triangles represent global unfolding rate constants determined by HX for chains A and B, respectively. The solid line through the data is a linear fit to the dependence of the global unfolding rate constants measured by fluorescence change on denaturant concentration. The dashed line through the data is a global linear fit of the dependence of global unfolding rate constants measured by HX on GdnHCl concentration. The error bars show the standard deviations in the data obtained from two independent measurements.

mass distributions of chain A and chain B. [Figure S9](#) shows that the simplest five-state scheme satisfactorily accounts for the data.

ETD fragmentation of the intact protein

Electron transfer dissociation (ETD) of intact dcMN was carried out subsequent to HX, in order to obtain high-resolution, segment-specific structural information. ETD generates c ions (N-terminal peptide fragments) and z ions (C-terminal peptide fragments) by the breakage of the N-C _{α} bond,⁴⁸ with minimal hydrogen scrambling.⁴⁹ As dcMN is composed of two non-covalently bound chains, which get separated from each other during the chromatographic run, the chains were fragmented sequentially and the peptides were identified. Reliably identified c and z ions were mapped on to the sequence of the protein ([Figure S10](#)). Four ions from each chain were considered, in order to determine the patterns of HX into the different sequence segments. Individual sequence segments, into which the extent of exchange was determined, are listed in Table S2.

Kinetics of HX into different sequence segments in zero denaturant

In the absence of denaturant, the sequence segments of chain B, 1–5 (β 1), 6–13 (loop between β 1 and α 1 and N-terminal of α -helix), 14–25 (α -helix), 26–35 (loop between α 1 and β 2) and 36–51 (β 2), represented by the c4, c34, z37 and z26 ions, respectively, opened up non-cooperatively as evident by the gradual shift of the mass spectra from high mass to low mass, with time of HX ([Figure S11](#)). The sequence segments of chain A, 52–56 (short loop before β 3), 64–76 (β 4) and 77–96 (β 5), represented by the c4, z32 and z19 ions, respectively, also showed non-cooperative structure opening ([Figure S12](#)). However, the sequence segment 57–63 (β 3) represented by the c26 ion, showed cooperative structural opening as indicated by the bimodal mass distribution during the slowest phase of HX ([Figure S12](#)).

The shift of the centroid of the mass distributions of the individual fragments was measured as a function of time of HX, in order to determine the rate constants of the transient opening events. In

Table 1 Rate constants of HX in the absence of denaturant at pH 8, 25 °C^a

Sequence segment	Fast phase of non-cooperative exchange		Slow phase of non-cooperative exchange		Very slow phase of non-cooperative exchange		Slowest phase of cooperative exchange	
	Rate constant (x 10 ⁻² s ⁻¹)	Amplitude ^b	Rate constant (x 10 ⁻⁴ s ⁻¹)	Amplitude ^b	Rate constant (x 10 ⁻⁶ s ⁻¹)	Amplitude ^b	Rate constant (x 10 ⁻⁶ s ⁻¹)	No. of D
Intact chain B (1 – 51)	2.0 ± 0.2	6.0 ± 0.2	3.1 ± 1.0	4.5 ± 0.1	9.0 ± 1.3	4.0 ± 0.2	–	
1 – 5 (β1)	6.0 ± 2.6	0.5 ± 0.2	71.1 ± 22.2	0.3 ± 0.15	15.8 ± 11.5	0.06 ± 0.02	–	
6 – 13 (loop1 + N-term α-helix)	2.0 ± 1.5	1.2 ± 0.2	4.8 ± 2.2	0.3 ± 0.07	–		–	
14 – 25 (α-helix)	1.1 ± 0.6	1.6 ± 0.3	1.4 ± 0.6	2.1 ± 0.1	8.4 ± 2.8	2.2 ± 0.3	–	
26 – 35 (loop between α1 – β2)	4.6 ± 2.0	1.8 ± 0.6	–		–		–	
36 – 51 (β2)	2.0 ± 0.7	2.0 ± 0.4	5.8 ± 2.6	1.0 ± 0.3	9.0 ± 2.0	1.8 ± 0.1	–	
Mean rate^c	1.85		2.13		8.72		–	
Intact chain A (52 – 96)	0.6 ± 0.2	2.5 ± 0.5	2.5 ± 0.24	3.6 ± 0.4	9.0 ± 1.5	3.1 ± 0.3	3.4 ± 0.3	7 ± 1
52 – 56 (short loop before β3)	0.5 ± 0.5	0.3 ± 0.1	2.3 ± 2.3	0.2 ± 0.1	9.0 ± 1.0	0.3 ± 0.1	–	
57 – 63 (β3)							3.0 ± 0.2	6 ± 1
64 – 76 (β4)	0.6 ± 0.06	1.0 ± 0.14	2.4 ± 1.0	0.72 ± 0.2	6.0 ± 1.6	3.2 ± 0.15	–	
77 – 96 (β5)	0.72 ± 0.2	1.3 ± 0.2	1.7 ± 0.6	1.4 ± 0.1	7.0 ± 0.1	0.64 ± 0.1	–	
Mean rate^c	0.64		1.92		6.3		–	

^aThe values in the white and grey coloured rows were obtained for HX into chains B and A of dcMN, respectively.

^bValues correspond to the number of deuteriums undergoing exchange in each phase.

^cCalculated using Eq. (1) described in the Materials and Methods section.

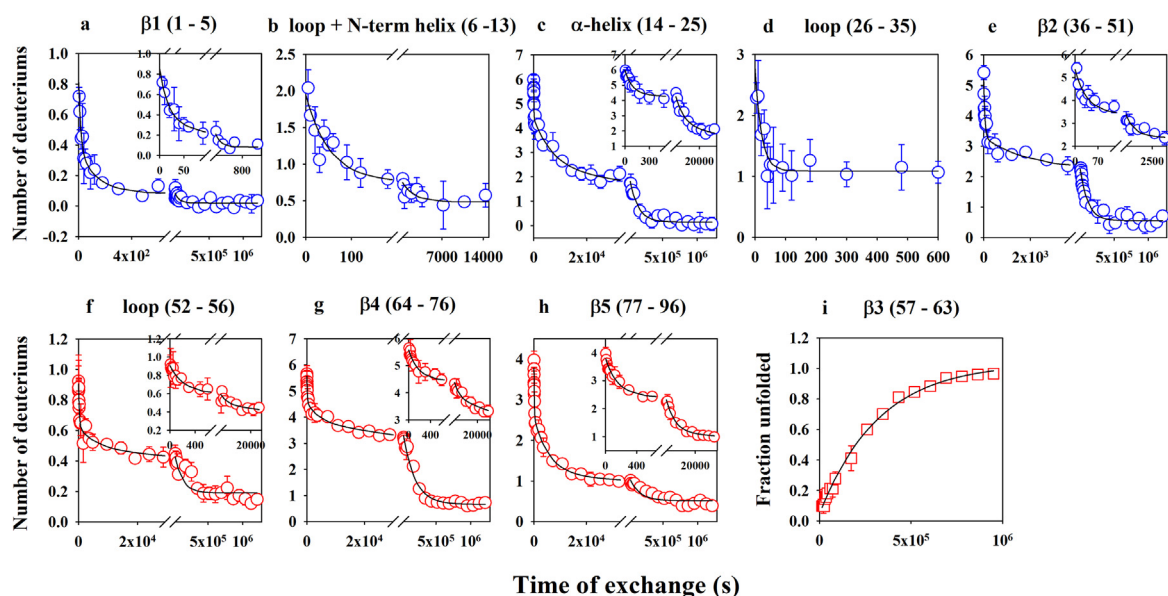


Figure 5. Kinetics of HX into different sequence segments of dcMN in the absence of denaturant at pH 8, 25 °C. Panels a, b, c, d, e, f, g, and h show the number of deuteriums retained as a function of time, by the sequence segments 1–5, 6–13, 14–25, 26–35, 36–51, 52–56, 64–76 and 77–96, respectively. The solid lines in all the panels represent a single, double or triple exponential fit to the data. The insets show the first two phases of HX for those sequence segments into which exchange occurs in three kinetic phases. The number of deuteriums retained by each sequence segment at any time of HX were calculated in a similar manner as was done for the intact protein (see methods). Panel i shows the increase in the fraction of the completely exchanged segment, 57–63, with time. The solid line through the data is a fit to a single exponential equation. The relative amounts of the completely exchanged segment were obtained by deconvolution of the bimodal mass distributions shown by the c26 ion that spans the β 3 strand of chain A. The kinetic parameters obtained from the fits are listed in Table 1. The error bars represent the standard deviations in the data obtained from three independent experiments.

the case of the fragment that showed bimodality, the bimodal mass distribution was deconvoluted to high mass and low mass distributions, and the increase in the fractional area under the low m/z peak was measured in order to determine the transient structure opening rate constant of that fragment. The kinetic parameters of the transient opening events of different sequence segments in the absence of denaturant are listed in Table 1. For each chain, the sum of the deuteriums retained in the ETD fragments at 5 s of HX matched the number of deuteriums retained in the intact chain. This suggested that no scrambling of the amide deuteriums happened during the fragmentation of the protein inside the mass spectrometer. Moreover, the total number of deuteriums that exchanged out in each kinetic phase from individual segments of a particular chain, matched the number of deuteriums that exchanged out from the intact chain (see Table 1).

Intact chain A exchanged out in three non-cooperative phases and one cooperative phase, while intact chain B exchanged out in three non-cooperative phases in the absence of denaturant (Figure 2). The sequence segments of chains A and B also opened up in multiple kinetic phases.

The sole α -helix and β 2, β 4 and β 5 unfolded in three non-cooperative kinetic phases, and the short loops, 6–13 and 26–35, exchanged out in two and one kinetic phases, respectively. Although β 1 (1–5) and short loop 52–56 opened up in three kinetic phases, the majority of their deuteriums were lost only in the fast kinetic phase. The remaining β -strand, β 3, exchanged out in the slowest cooperative phase of HX (Figure 5).

The mass distributions of the c4, z32 and z19 ions of chain A were unimodal at all times of exchange, while only the c26 ion showed a bimodal mass distribution (Figure S12). When the sequences of these ions were mapped on to the sequence of the protein, it was evident that only the residues of the β 3 strand opened up in a correlated manner in the slowest phase of HX (Figure 5(i)). The rate constant of this cooperative phase also agreed well with the rate constant of the global unfolding phase of intact chain A. The number of deuteriums undergoing exchange in the cooperative phase was also the same for the c26 ion and the intact chain A (Table 1). Hence, the slowest opening residues were found to be located in the β 3 strand, and exchanged out only during the global unfolding of the protein.

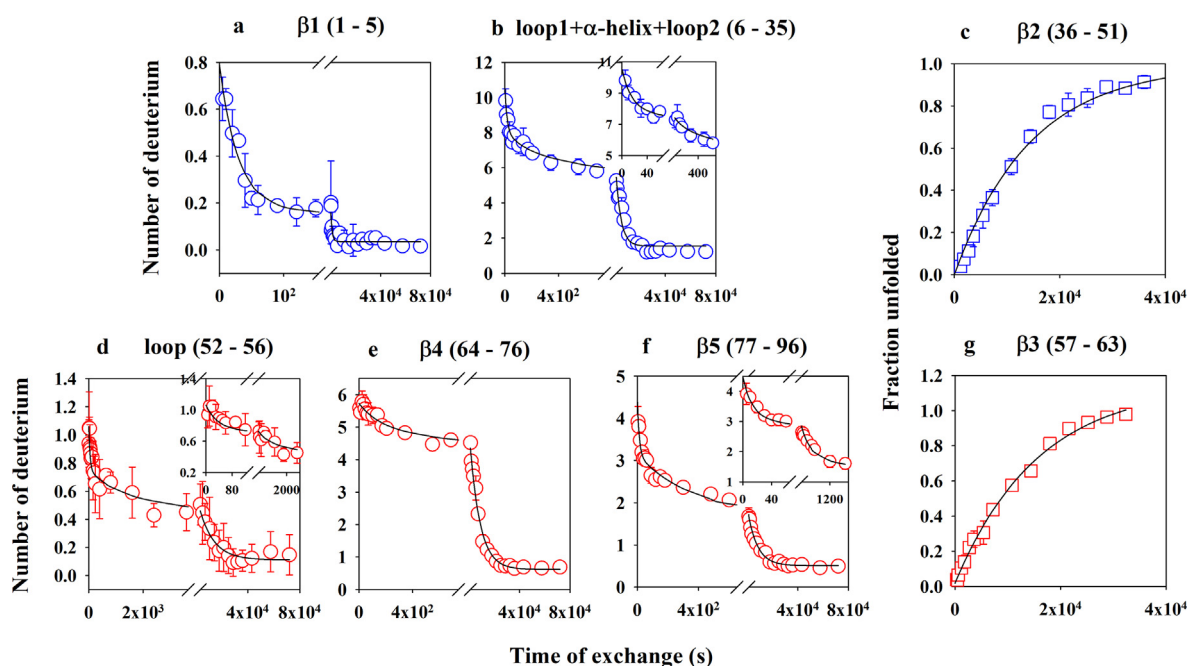


Figure 6. Kinetics of HX into different sequence segments of dcMN in the presence of 1 M GdnHCl at pH 8, 25 °C. Panels a, b, d, e and f show the number of deuteriums retained as a function of time by the sequence segments 1–5, 6–35, 52–56, 64–76 and 77–96, respectively, whereas panels c and g show the increase in the fraction of completely exchanged segments, 36–51 and 57–63, with time. The solid lines through the data in all the panels represent either a single (c and g) or double (a and e) or triple (b, d and f) exponential fit to the data. The insets show the first two phases of HX for those sequence segments into which exchange occurs in three kinetic phases. The number of deuteriums retained by each sequence segment at any time of HX was calculated in a manner similar to that for the intact protein (see methods). The relative amounts of completely exchanged segment were obtained by deconvolution of the bimodal mass distributions shown by the z37 (panel c) and c26 (panel g) ions that span the β 2 strand of chain B and the β 3 strand of chain A, respectively. The kinetic parameters obtained from the fits are listed in Table 2. The error bars represent the standard deviations in the data obtained from three independent experiments.

Kinetics of HX into different sequence segments in the presence of 1 M GdnHCl

The c4 and c34 ions from chain B showed a continuous shift in the mass distribution with time of HX in the presence of 1 M GdnHCl. But the z37 ion, which showed a unimodal mass distribution in the absence of GdnHCl, showed a bimodal mass distribution (Figure S13(a)). Hence, in the presence of 1 M GdnHCl, the exchange rate constant of a group of sequence segments had to be considered, instead of the individual sequence segments. Thus, the deuterium retention calculated for (c34–c4) covered the sequence segment 6–35, which includes the loop between β 1– α 1, α 1, and the loop between α 1– β 2. Sequence segment 1–5 (β 1) unfolded in two non-cooperative kinetic phases (Figure 6(a)). Sequence segment 6–35 exchanged out in three non-cooperative kinetic phases (Figure 6(b)) whose rate constants agreed well with the rate constants of HX into intact chain B. The rate constants of these three phases, as well as the number of deuteriums that exchanged out in each

phase of HX, were also comparable for intact chain B and its sequence segments (Table 2).

The β 2 strand exchanged out cooperatively in the slowest phase of HX in the presence of 1 M GdnHCl. The c34 and z37 ions share residues 14–35. The c34 ion showed a unimodal shift in its mass spectra for the entire time of HX, while the z37 ion showed bimodal mass distributions, indicative of cooperative opening (Figure S13(a)). Figure 6(c) shows the appearance of the U population with time of HX; the rate constant of this phase also agreed well with that of the global unfolding phase of chain B (Table 2). 4 ± 1 deuteriums were lost from β 2 in a concerted manner during global unfolding.

In the case of chain A, the sequence segments exchanged out in a manner similar to that in the absence of denaturant. Sequence segments 52–56 and 77–96 lost their protection in three non-cooperative kinetic phases (Figure 6(d) and (f)), while sequence segment 64–76 exchanged out in two non-cooperative kinetic phases (Figure 6(e)).

Sequence segment 57–63 (β 3) was found to open up in a correlated manner in the slowest

Table 2 Rate constants of HX in the presence of 1 M GdnHCl at pH 8, 25 °C^a

Sequence segment	Fast phase of non-cooperative exchange		Slow phase of non-cooperative exchange		Very slow phase of non-cooperative exchange		Slowest phase of cooperative exchange	
	Rate constant (x 10 ⁻² s ⁻¹)	Amplitude ^b	Rate constant (x 10 ⁻⁴ s ⁻¹)	Amplitude ^b	Rate constant (x 10 ⁻⁶ s ⁻¹)	Amplitude ^b	Rate constant (x 10 ⁻⁶ s ⁻¹)	No. of D
Intact chain B (1 – 51)	9.0 ± 3.0	3.1 ± 0.2	76.4 ± 30.0	3.3 ± 0.6	344.0 ± 54.7	3.8 ± 0.4	63.5 ± 10.2	4 ± 1
1 – 5 (β1)	3.5 ± 1.3	0.6 ± 0.1	9.4 ± 3.8	0.15 ± 0.03	–		–	
6 – 35 (loop 1 + α-helix + loop 2)	7.0 ± 1.2	2.5 ± 0.4	65.0 ± 15.3	1.4 ± 0.4	250.0 ± 50.0	5.2 ± 0.3	–	
36 – 51 (β2)							70.0 ± 6.0	4 ± 1
Mean rate^c	6.0		41.34		–		–	
Intact chain A (52 – 96)	8.0 ± 4.4	1.5 ± 0.4	55.3 ± 7.3	2.8 ± 0.1	196.0 ± 13.0	3.7 ± 0.3	100.9 ± 2.2	7 ± 1
52 – 56 (short loop before β3)	2.9 ± 1.0	0.3 ± 0.1	15.7 ± 10.0	0.2 ± 0.12	90.2 ± 10.1	0.5 ± 0.04	–	
57 – 63 (β3)							63.8 ± 4.1	7 ± 1
64 – 76 (β4)	–		70.2 ± 12.4	0.8 ± 0.2	125.6 ± 2.6	4.3 ± 0.1	–	
77 – 96 (β5)	8.0 ± 1.3	1.4 ± 0.3	30.2 ± 8.0	1.3 ± 0.2	131.4 ± 42.2	1.4 ± 0.3	–	
Mean rate^c	6.1		34.2		123.0			

^aThe values in the white and grey coloured rows were obtained for HX into chains B and A of dcMN, respectively.

^bValues correspond to the number of deuteriums undergoing exchange in each phase.

^cCalculated using Eq. (1) described in the Materials and Methods section.

phase of exchange (Figure S13(b)) with a rate constant that agreed well with the global unfolding rate constant (Figure 6(g)). The number of deuteriums (7 ± 1) that exchanged out from the β3 strand during the slowest phase of HX also remained the same in both the absence and

presence of denaturant. The global unfolding rate constants measured for both the segments 36–51 (β2) and 57–63 (β3) were also in very good agreement with each other (Table 2).

For each kinetic phase of HX into chain B and chain A in the intact protein, measured in both the

absence and the presence of GdnHCl, the mean rate constant, calculated from the exchange rate constants of the different segments, agreed well with the rate constant of exchange measured into the chains in intact protein (Tables 1 and 2). For each kinetic phase, the exchange rate constants of the individual sequence segments were not identical but were dispersed around the mean rate constant (Tables 1 and 2), suggesting that different sequence segments did not lose structure in a synchronous manner.

Discussion

dcMN undergoes HX in the EX1 regime

The observed rate constants of HX will be the rate constants of transient unfolding only when HX occurs in the EX1 regime (see SI text). The observation that the rate constants of the fast and slow non-cooperative phases of exchange of both the chains are independent of pH in the range 7–9 (Figure S1), suggests that the protein undergo HX in the EX1 regime for these phases of exchange. The rate constants of the very slow non-cooperative phase of both the chains, as well as the cooperative phase of chain A, show only a 2-fold increase with an increase in pH from 7 to 9, which is insignificant in comparison to the expected 100-fold increase if HX were in the EX2 regime.^{45,50} It is likely that the small increase in the rate constants of exchange of the two slowest phases with an increase in pH is due to the

decreased stability of dcMN at higher pH.³⁴ The appearance of bimodal mass spectra at the later phase of exchange also confirms that HX occurs in the EX1 regime. In fact, HX was expected to occur in the EX1 regime, because k_{int} (43.3 s^{-1}) is more than 280-fold faster than the closing (folding) rate constant, k_{cl} (0.15 s^{-1}) at pH 7 (see SI). At pH 8, the folding rate constant is the same as at pH 7, and HX is even more likely to be in the EX1 regime. In a previous study, it was observed that MNEI, the single chain homolog of dcMN, also undergoes HX in the EX1 regime at pH 8, 25 °C.^{10,23} In the presence of 0.2–1 M GdnHCl, k_{cl} for dcMN will be even slower; hence, HX will continue to be in the EX1 regime.

Structural loss initially occurs via a multitude of incremental structure opening events

The observation (Figures 2 and 3) that mass spectra shift continuously with time of exchange, both in the absence and presence of GdnHCl, suggests that 1–2 amide sites open up to HX at a time. In other words, the continuous shift in the peak of the mass distribution is suggestive of gradual (barrier-less) structural change. The very large number of crossover points of the mass distributions (Figures 2 and 3) confirms that structure opening to HX occurs incrementally via a multitude of steps that make it close to being continuous in nature.

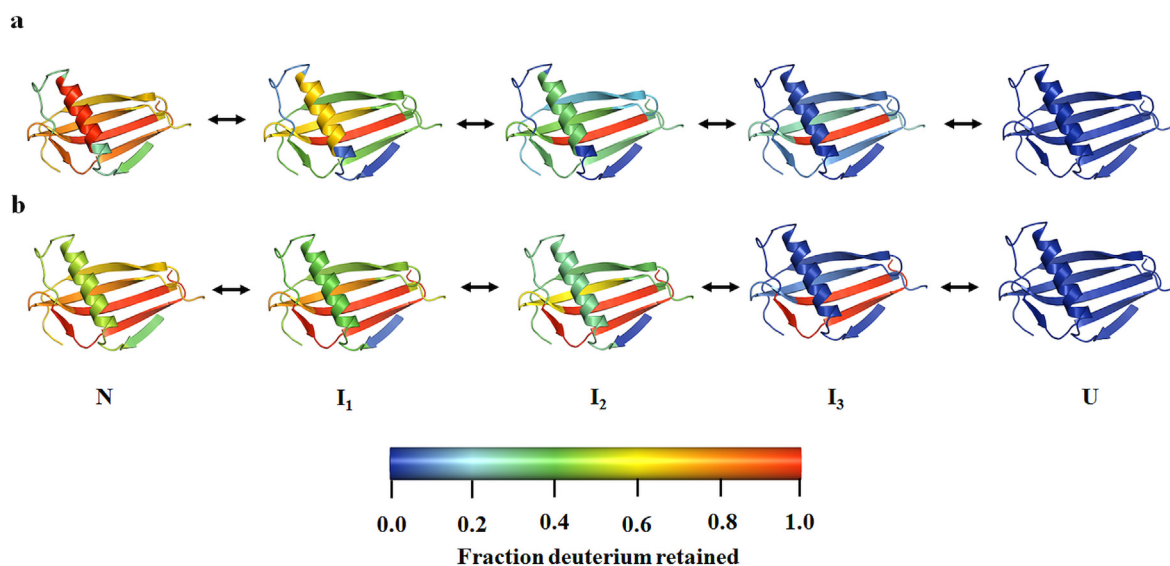


Figure 7. Structural change during transient unfolding. The fraction of deuterium retained, which represents the fractional structural change yet to occur, has been mapped on to the structures of native dcMN for the N state (at 5 s of exchange), the U state (at 12 days of exchange) and the partially unfolded intermediates populated at the end of each kinetic phase of HX in the absence (a) and presence (b) of denaturant. The separation of the two chains during the I₃ ↔ U transition is not shown. The colour bar at the bottom indicates the fraction of deuterium retained in the different secondary structural elements. The structures of dcMN were drawn using the Pymol software and the PDB file ID 3MON.

Gradual unfolding occurs in three sequential non-cooperative kinetic phases followed by cooperative global unfolding

Gradual unfolding has been shown to be interrupted by three kinetic pauses (Figure 4(a)), at each of which a high energy intermediate, I_1 , I_2 or I_3 , is populated transiently (Figure S9). The observation that the logarithm of the rate constant of each phase increases significantly with an increase in GdnHCl concentration (Figure 4(a)) indicates that I_1 , I_2 and I_3 are the products of specific structural transitions that cause significant change in surface area, rather than of local fluctuations, for which a lack of dependence on the denaturant concentration of the rate constants is expected.^{51,52} The fast phase is 50 to 100-fold faster than the slow phase which is 50 to 100-fold faster than the very slow phase, even in 1 M GdnHCl where about 87 % of the protein molecules are unfolded at equilibrium (Figure S2). It is therefore unlikely that I_1 , I_2 and I_3 form in competition with each other on multiple pathways, because then the flux of molecules unfolding to U would predominantly occur *via* I_1 . In support of the intermediates being transiently populated in the absence of denaturant, the plot of the logarithm of the observed rate constants of unfolding, measured by both HX and fluorescence, *versus* GdnHCl concentration, shows a kink at low (~ 0.4 M) GdnHCl concentration (Figure 4(b)). Such kinks denoting the population of kinetic unfolding intermediates in native-like conditions have also been seen for several other proteins.^{10,53–56}

The similarity in the rate constants of the three non-cooperative phases of exchange for chain A and chain B (Figure 4(a)), indicates that both the chains remain associated with each other as the protein unfolds to intermediates I_1 , I_2 and I_3 , which must therefore be dimeric intermediates. All protection against HX is lost during the slowest cooperative phase, as I_3 unfolds to U, because, presumably, the two chains dissociate transiently during this phase, and the individual chains possess no structure³⁴ that affords protection. For several other proteins, including the RNase H,⁴⁴ turkey ovomucoid third domain,^{57,58} barstar,⁵⁹ ubiquitin,⁶⁰ RNase A⁶¹ and thioredoxin,⁶² it has also been observed that the slowest exchanging amide sites require global unfolding of the protein to occur, before they can undergo exchange.

Structural mechanism of unfolding

The capability to determine the time course of exchange into each segment of both chain B and chain A (Tables 1 and 2) for which a fragment could be generated after HX by ETD, allowed the structure opening events to be described, most simply, by a $[N \leftrightarrow I_1 \leftrightarrow I_2 \leftrightarrow I_3] \leftrightarrow U$ mechanism

(see SI). The HX data were found to fit well to this simple mechanism (Figure S9). It became possible then to determine a structural mechanism for unfolding in 0 M GdnHCl (Figure 7(a)) and in 1 M GdnHCl (Figure 7(b)).

The structural mechanism determined for dcMN (Figure 7) stands in stark contrast to that suggested for cytochrome c,^{6,50} RNase H⁴⁴ and moPrP.⁶³ For all of these other proteins, each structural unit (foldon) apparently loses all its structure independently in only one step, and the foldons appear to lose their structure in a sequential manner. For several other proteins, including barstar,⁵⁹ thioredoxin,⁶² T4 lysozyme,⁶⁴ human PrP⁶⁵ and mouse Dpl⁶⁶ foldons have not been observed in HX NMR studies. It appears that natural selection has provided multiple solutions to how structure can develop in protein folding reactions not just across different proteins, but also for the same protein.³⁷ Evolution has ensured robustness in folding by allowing for different mechanisms for structure to assemble.

In the case of dcMN, the data preclude the existence of foldons. On the contrary, each secondary structural unit unfolds in more than one kinetic phase. It appears that the structure in each secondary structural unit is stabilized by multiple specific tertiary (packing) interactions, which break sequentially in three kinetic phases.^{12,23} Hence, all the structure in a secondary structural unit cannot be lost in one cooperative step. The alternative explanation is that dcMN utilizes multiple pathways to unfold, and that each secondary structural unit is lost in a different step on each pathway. Indeed, the folding of dcMN has been shown to occur *via* multiple pathway.⁶⁷ Moreover, in the case of the single chain variant MNEI, multi-site FRET studies³⁷ have shown that the same structure may be lost early on one folding pathway and late on another.

Unfolding in the absence of denaturant

Native-state HX studies,^{6,7,10,23,40,41,43,44,58–62,68,69} such as the current study, reveal how folding occurs under physiological conditions in the absence of any denaturant. In this study using HX-MS, the structural mechanism of unfolding has been elucidated both in the presence and in the absence of chemical denaturant (Figures 7 and S9). While the kinetic mechanism is the same, the structures of the intermediates are different at zero and low denaturant concentrations (Figure 7): secondary structural elements are lost at different stages of unfolding, as also seen in the case of other proteins.^{23,40} The sequence of structure formation during folding will be the exact opposite of the sequence of structure loss during unfolding under identical conditions. Hence, the current study indicates that the structures of folding intermediates are modulated by chemical denaturant. This result is important because most studies of protein folding are carried out in the presence of denaturant, and

thus the structural mechanism elucidated might be different from that which would apply under physiological conditions in the absence of any denaturant.

dcMN as a model for binding-induced folding

The folding of dcMN is an example of a binding-induced folding reaction: the individual chains of dcMN do not possess any structure in isolation,³⁴ and acquire structure only after forming an encounter complex.⁶⁷ Many partially or completely unfolded proteins, as well as intrinsically disordered proteins, fold and acquire structure upon ligand binding, in order to function in physiological conditions.^{70,71} For example, the unfolded PI3K SH3 domain folds in the presence of a proline-rich peptide.⁷² The current study, showing that the folding of dcMN occurs *via* progressively more structured folding intermediates, therefore suggests that many binding-induced folding reactions may occur in multiple steps, and raises the possibility that the intermediate forms that are populated may themselves have physiological function because they possess partial native-like structure.

Modulation of cooperativity upon addition of denaturant

Earlier studies with both MNEI and the PI3K SH3 domain had shown how the cooperativity of unfolding can be modulated by changing the relative stabilities of the N and U states and the transition state, either by addition of denaturant or osmolyte, or by changing the pH, or by mutation.^{10,23,39–41} In this study, it is shown that the size of the cooperatively unfolding unit of dcMN becomes larger when the protein is destabilized upon the addition of GdnHCl (Figures 2 and 3). It

is perhaps because of the greater hydrophobicity (Figure S14(a)) and deeper burial (Figure S14(b)) of the residues in β_3 compared to those in β_2 , that β_3 opens up cooperatively in the slowest phase of exchange in native and native-like conditions. The strongly protected residues in LysN,⁶⁸ ubiquitin⁶⁰ and cold shock protein⁶⁹ also appeared to be more hydrophobic.

In the presence of 1 M GdnHCl, 4 ± 1 deuteriums in β_2 , which are protected in I_3 , exchange out during the $I_3 \leftrightarrow U$ step in an all-or-none manner (Figure S13(a) and Table 2). Thus, the structure of I_3 , from which cooperative exchange occurs, is different in the absence and presence of denaturant. β_2 is not protected against HX in I_3 in 0 M denaturant, but is protected in the presence of 1 M GdnHCl (Figure 7). Surprisingly, the 4 amide deuteriums in β_2 that lose their protection only during the slowest cooperative phase of unfolding in 1 M GdnHCl include 3 that lose their protection earlier in the fast and slow phases of transient unfolding in 0 M GdnHCl. The observation that 3 amide deuteriums in β_2 exchange out 100–1000 fold slower in 1 M than in 0 M GdnHCl, was unexpected because the denaturant should have promoted faster unfolding. It suggests that GdnHCl smoothens the energy barriers by slowing down the fast and slow phases of exchange into β_2 in such a manner that the effective barrier for these 3 deuteriums to exchange out is increased.²³

Comparison of the unfolding cooperativity of dcMN and MNEI

The structures of dcMN and MNEI are virtually identical to each other (Figure 1). In the case of

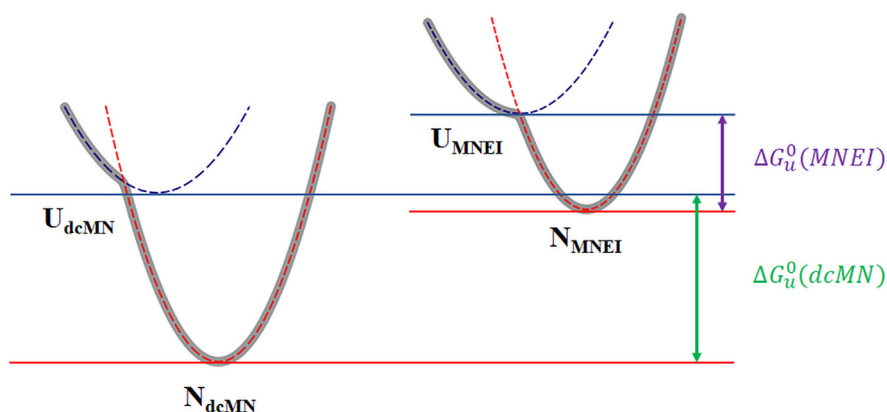


Figure 8. Comparison of the free energy surfaces of dcMN and MNEI in native conditions. The red and blue dashed lines represent the N and U energy wells of the proteins, respectively. The point of intersection of the N and U energy wells along the reaction coordinate is the position of the transition state. The resultant free energy surfaces are denoted by the grey lines and were drawn according to the equation, $G = -\ln [\exp\{-y_U(x)\} + \exp\{-y_N(x)\}]$, where $y_U(x)$ and $y_N(x)$ are the parabolic functions describing the free energies of the U and N wells, respectively, and x is the horizontal variable. The barrier-limited transition, between the N and U energy wells for dcMN, becomes barrierless for MNEI, as a consequence of the relative extents to which the N and U states are destabilized in the latter compared to in the former.

MNEI, exchange is completely non-cooperative in the absence of denaturant.¹⁰ In contrast, 7 ± 1 deuteriums exchange out cooperatively in the slowest phase of exchange in the case of dcMN in the absence of denaturant (Figure 2 and Table 1). In the case of destabilized mutant variants of MNEI too, 7 amide deuteriums exchange out cooperatively in the slowest phase in the absence of denaturant and were shown to belong to the sequence stretch Pro41–Ala67 which spans $\beta 2$ and $\beta 3$,³⁹ but it had not been possible to determine whether they belonged to $\beta 2$ or $\beta 3$.^{23,39} In the case of dcMN, $\beta 2$ is part of chain B, while $\beta 3$ is part of chain A. Since only the chain A component of dcMN shows cooperative HX in the absence of denaturant, and since the number of cooperatively exchanging amide deuteriums (7 ± 1) matches the number of cooperatively exchanging amide deuteriums in the destabilized MNEI variants, it is likely that the cooperatively exchanging deuteriums belong to $\beta 3$ and not to $\beta 2$.

When HX occurs in the presence of 1 M GdnHCl, MNEI and its destabilized variants all have 14 deuteriums exchanging out during the slowest cooperative phase.³⁹ The observation that the number of cooperatively exchanging amide deuteriums remains at 7 ± 1 in chain A in 1 M GdnHCl in the case of dcMN (Table 2), indicates that these additional 7 amide deuteriums are likely to belong to $\beta 2$ in MNEI. Indeed, 4 ± 1 amide deuteriums of $\beta 2$ exchange out cooperatively from dcMN in the presence of 1 M GdnHCl (Table 2).

It has been suggested that the cooperative folding observed for small naturally occurring proteins is a product of natural selection, and it has been observed that small designed proteins have limited folding cooperativity.^{73–78} While dcMN is a product of natural selection, MNEI is an artificially constructed variant. It would appear therefore that the folding of dcMN is more cooperative than that of MNEI because evolutionary pressures that modulate protein function and stability also modulate protein folding cooperativity.

Kinetic cooperativity depends on thermodynamic stability

Figure 8 shows how the difference in stabilities of dcMN and MNEI at the standard state concentration of 1 M could account for the difference observed in the cooperativities of their unfolding transitions: the differences in the stabilities of their N and U states could make the unfolding of MNEI barrier-less and the unfolding of dcMN barrier-limited, in native and native-like conditions (0–0.4 M GdnHCl). The U state of MNEI is less stable than that of dcMN because of entropic reasons: it has one chain while dcMN has two chains. The N state of MNEI also appears to be less stable than that of dcMN. Either the covalent linkage of the two chains introduces strain into, and destabilizes the N state of MNEI, or the additional two mobile free ends of

chains A and B entropically stabilize the N state of dcMN. Not surprisingly, the structure of dcMN affords protection against HX to fewer amide sites than does that of MNEI, and the amide sites protected in dcMN undergo exchange faster than those protected in MNEI.³⁹

In the absence of any denaturant, the transient unfolding of MNEI to the U state occurs completely *via* three non-cooperative kinetic phases, while the transient unfolding of dcMN occurs *via* three non-cooperative kinetic phases and one cooperative kinetic phase. In the case of MNEI, it appears that gradual barrier-less unfolding pauses at the end of each kinetic phase, because a specific packing interaction with a high barrier has to be disrupted before gradual unfolding can resume.^{12,23} It is likely that the origin of the three non-cooperative kinetic phases seen for dcMN is similar, but it is not known at present why in the case of dcMN there is an additional barrier-limited step that retards gradual unfolding. Nor is it known why $\beta 3$ loses structure non-cooperatively in MNEI but cooperatively in dcMN. It seems that the relative energies of the intermediates and transition states are modulated in dcMN, because of its greater overall stability, in such a manner that its folding is more cooperative than the folding of MNEI.

It should be remembered that comparing the stability of heterodimeric dcMN to that of monomeric MNEI is not straightforward. The free energy of unfolding of MNEI is independent of protein concentration. On the other hand, the dissociation and unfolding of dcMN become more favorable as the protein concentration is lowered, in accordance with the Le Chatelier's principle; hence, the free energy of unfolding will decrease at lower protein concentration. The free energy of unfolding of dcMN is $11.4 \text{ kcal.mol}^{-1}$ at the standard concentration of 1 M (Figure S2). It decreases by $\sim 7 \text{ kcal.mol}^{-1}$ when such a standard solution is diluted by a factor of 10^5 to $10 \mu\text{M}$,^{79,80} which is the protein concentration at which the HX reaction was carried out. Since the free energy of unfolding of $10 \mu\text{M}$ dcMN is less than that of MNEI, it is not surprising that the size of its cooperative unfolding unit, comprising 7 amide sites in the absence of denaturant, matches that seen for destabilized mutant variants of MNEI.³⁹ Future studies will focus on obtaining a better understanding of the correlation between stability and cooperativity in the case of dimeric proteins.

Conclusion

The present HX-MS study structurally delineates the cooperative and non-cooperative transitions associated with the unfolding of the naturally occurring heterodimeric variant of monellin under native and native-like conditions, as well as under mildly denaturing conditions. The mechanism of

unfolding is found to be the same both in the absence and presence of denaturant. Chain A unfolds in a cooperative manner while chain B unfolds in a noncooperative manner in strongly native conditions (≤ 0.4 M GdnHCl). However, the extent of the cooperativity of unfolding increases upon the addition of mildly denaturing concentrations of GdnHCl (0.6–1 M), where chain B also exchanges out cooperatively along with chain A. An analysis of HX into different structural segments suggested that the $\beta 2$ and $\beta 3$ strands, comprising the core of the protein, unfold in the slowest cooperative phase. The unfolding of dcMN is more cooperative than that of MNEI, which has been rationalized on the basis of their relative free energies of unfolding.

Materials and Methods

Protein expression and purification

Double chain monellin was purified according to the protocol described previously.⁸¹ The purity of the protein was checked by electrospray ionization mass spectrometry (ESI-MS) and found to be >95%. The masses of the two chains, determined by ESI-MS, were found to be 5965.2 Da and 5382 Da for chain B and chain A, respectively, as expected. The concentration of the protein was determined by measuring the absorbance at 280 nm, using an absorbance coefficient value of $14,600 \text{ M}^{-1} \text{ cm}^{-1}$.

Buffers and reagents

All the reagents used here in this study were of high purity grade, and were purchased from Sigma. Ultra-pure GdnHCl was obtained from United States Biochemicals, and was of the highest purity grade. All the HX experiments were carried out at 25 °C. Sodium phosphate buffer (20 mM), Tris buffer (20 mM) and Glycine-NaOH buffer (50 mM) were used for the labelling reaction at pH 7, pH 8 and pH 9, respectively. Ice-cold 100 mM Glycine-hydrochloride buffer containing 8 M GdnHCl at pH 2.2 was used as the quenching buffer to stop the labelling reaction. The concentration of GdnHCl in each buffer was determined by measuring the refractive index of the solutions using an Abbe refractometer. The pH values reported for D₂O buffers have not been corrected for any isotope effect.

Fluorescence monitored equilibrium and kinetic unfolding studies

GdnHCl-induced equilibrium and kinetic unfolding of dcMN was monitored using a stopped-flow module (SFM4) attached to the MOS-450 optical system from Biologic, as described previously.³⁴ An excitation wavelength of 280 nm was used, and the fluorescence emission was collected at

340 nm using a 10 nm band-pass filter from Asahi Spectra. The final protein concentration was 10 μM .

Deuteration of dcMN

Deuteration of dcMN was carried out according to the protocol described previously for MNEI.¹⁰ Briefly, the lyophilized protein was dissolved in D₂O buffer (10 mM Tris, pH 8.2) to a final concentration of 200 μM . The pH of the solution was then increased to 12.8 by the addition of 1 N NaOD, and the protein was incubated for 5 min. Then the pH of the solution was dropped directly to 1.6 by the addition of 1 N DCl. Finally, the pH was made up to 8 by gradual addition of NaOD. dcMN unfolds at high pH (12.8) and all of its amide sites get exposed and undergo exchange with solvent deuteriums. The mass of the fully deuterated protein was checked by injecting it directly into the mass spectrometer and found to be the same every time. Also, the CD spectrum of refolded, deuterated protein confirmed that the structure of the protein did not get significantly affected by the pH jumps (Figure S15). For ETD experiments, the deuteration procedure was carried out at 400 μM final protein concentration.

HX kinetics

For carrying out HX into the intact protein, 7 μl of deuterated protein in D₂O buffer (10 mM Tris, pH 8.2) were mixed with 133 μl of protonated labelling buffer (20 mM Tris, pH 8). The final protein concentration during exchange was 10 μM . At different times of exchange, 125 μl of the exchange reaction were mixed with 375 μl of quenching buffer (100 mM Gly-HCl, 8 M GdnHCl, pH 2.2) on ice to stop the exchange reaction. After quenching, the final pH of the reaction became 2.6, and the final concentration of GdnHCl was 6 M. The samples were incubated for 1 min under these quenching conditions. For the back-exchange control, deuterated labelling buffer was used instead of protonated labelling buffer. The back-exchange control sample was examined to determine the number of deuteriums lost during the sample processing. These deuteriums were weakly protected and exchanged out rapidly.

Electron transfer dissociation (ETD) was used to generate fragments of the protein subsequent to exchange. For the fragmentation experiment, a final protein concentration of 20 μM was used. The higher protein concentration helped to achieve a better ion count of peptide fragments obtained from ETD. GdnHCl was added to the quenching buffer to unfold the protein as it also increased the ion count upon ETD fragmentation. The concentrations of GdnHCl in the labelling buffers and quenching buffers were adjusted as required when the exchange reactions were carried out at different final concentrations of GdnHCl (0.2–1 M).

Sample processing for mass spectrometry

After quenching and incubation for 1 min, the reaction mixture was desalted using a Sephadex G-25 Hi-trap desalting column from GE, equilibrated with ice-cold acidic water at pH 2.6 (pH was adjusted using formic acid) attached to either an AKTA basic HPLC system (GE Healthcare) or a Postnova AF4 system. The desalted sample was then injected into the HDX module coupled to a nanoAcquity UPLC (from Waters Corporation), and analyzed using a Synapt G2 HD mass spectrometer (Waters Corporation). The protein was first loaded on to a C18 reverse phase trap column using water containing 0.05% formic acid at a flow rate of 100 $\mu\text{l}/\text{min}$ for 1 min. The elution of the two chains of the protein from the column was done using a gradient of 35–95% acetonitrile (0.1% formic acid) at a flow rate of 40 $\mu\text{l}/\text{min}$ in 3 min. The temperature of the entire chromatography assembly was maintained at 4 °C inside the HDX module (Waters Corporation) to minimize the back exchange during the processing of the sample.^{82,83}

For carrying out ETD, the desalted protein was injected into the HDX module coupled to a nanoAcquity UPLC. The protein was first trapped in a trap column with water containing 0.05% formic acid at a flow rate of 100 $\mu\text{l}/\text{min}$ for 1.5 min. Chains A and B were separated using an analytical column (C18 reverse phase), with a gradient of 35–55% acetonitrile containing 0.1% formic acid, in 9 min. The separation of the two chains was necessary as only one precursor mass could be allowed to undergo ETD fragmentation at a time.

Data acquisition parameters

The source parameters were set to the following values for ionization: capillary voltage, 3 kV; sample cone voltage, 40 V; extraction cone voltage, 4 V; source temperature, 80 °C; and desolvation temperature, 200 °C. In between two consecutive sample runs, 2–3 blank runs were carried out by injecting only distilled water to minimize the carry-over from the previous run.

1,4-dicyanobenzene was used as the ETD reagent to fragment the intact protein. The radical anions were generated from the ETD reagent using a glow discharge current of 35 μA , and a makeup gas (nitrogen) with flow rate of 35 ml/min was used to obtain reagent ion counts of $> 10^6$ per scan. The + 7 charge states for both the chains A and B were used to achieve optimum fragmentation. The other instrument parameters were set to the following values: trap wave velocity, 350 m/s; trap wave height, 0.5 V. Source parameters values were set to those mentioned above for the intact protein. The transfer collision energy was ramped from 10 eV to 14 eV in order to achieve higher ion counts of the fragment ions.

One precursor mass (+7 charge state for both the chains) from each chain was allowed one after another to undergo ETD fragmentation inside the trap cell for ~ 60 s, and the fragmentation data for the two chains were collected in two channels.

The sample cone voltage, which has to be adjusted correctly to prevent the scrambling of deuteriums prior to fragmentation,⁴⁹ was set to 40 V. This voltage was chosen because a previous study with MNEI, using the same mass spectrometer, had shown that scrambling did not occur when the sample cone voltage was in the range of 10–60 V.²³ Fragmentation of dcMN was also carried out at different sample cone voltages ranging from 30 to 50 V, and the fragments did not show significant differences in their deuterium retention across the range of sample cone voltage used (data not shown). This indicated that scrambling did not occur in this condition.

Data analysis

(a) *Analysis of intact protein.* The protein mass spectrum at each timepoint was generated by combining 40 scans, each 1 s long, from the elution peak of the total ion count (TIC) chromatogram. Each mass spectrum was then processed further by background subtraction and smoothing using the MassLynx version 4.1 software (Figure S16). The highest intensity peak (the + 7 charge state peak) for both chain A and chain B, from smoothed spectra, was taken for further analysis at every timepoint. The signal of the + 7 charge state peak was normalized by its total area at each timepoint using the Origin software. Then the mass distribution was fitted to either a single Gaussian equation if it was unimodal, or to the sum of two Gaussian equations if it was bimodal in nature, and the width(s), height(s) and centroid(s) of the mass distributions were determined. The number of deuteriums retained at a particular time point by both chain A and chain B was calculated by subtracting the protonated chain mass from the mass obtained from the centroid of the mass distribution. The rate constant of exchange (opening to HX) was determined by fitting the number of deuteriums retained *versus* the time of exchange plot to a single, double or triple exponential equation using the SigmaPlot software (v12.0). The fraction of completely unfolded protein was obtained by dividing the area under the lower m/z peak with the total area under the mass distribution.

(b) *Analysis of the fragments generated by ETD.* The mass spectra of the ETD fragments of chains A and B were generated by combining the elution peaks of the TIC chromatograms obtained separately for the two chains. The centroid mass spectra, obtained from these combined mass spectra, were analyzed using the Biolyx software to identify the individual c and z ions of both

chains. The masses of the individual ions were calculated from the intensity-weighted isotopic abundances, and the deuterium retained by each fragment at a particular time was determined in the same way as it was done for the intact protein. The extent of exchange at different sequence segments were determined by doing multiple subtractions with consecutive c and z ions. The operations are summarized in Table S2.

The width, height and centroid of the mass distribution of each ion generated by ETD were determined in the same way as was done for the intact protein (see above). The kinetic traces for HX into different sequence segments were also obtained and analyzed in the same way as was done for the intact protein (see above). The mean rate constant of HX for each kinetic phase of an individual chain, averaged over all its sequence segments, was calculated using following equation:

$$R = \frac{\sum \alpha_i}{\sum \alpha_i \tau_i} \quad (1)$$

where α_i is the amplitude of a particular kinetic phase, and τ_i is the time constant of the same kinetic phase of i -th fragment.

Kinetic simulations

To determine the kinetic mechanism of unfolding, the mass distributions of the +7 charge state at different times of exchange, for both chain A and chain B, were globally fit to a five state kinetic mechanism using the MATLAB software. The parameters of the kinetic mechanism were obtained by simulating mass distributions using the `fminsearchbnd` function. The process is described in detail in the SI methods.

CRedit authorship contribution statement

Rupam Bhattacharjee: Conceptualization, Methodology, Software, Writing – original draft, Validation, Formal analysis, Investigation. **Jayant B. Udgaonkar:** Conceptualization, Writing – review & editing, Validation, Visualization, Resources, Supervision, Funding acquisition.

DECLARATION OF COMPETING INTEREST

The authors declare that they have no known competing financial interests or personal relationships that could have appeared to influence the work reported in this paper.

Acknowledgements

We thank members of our laboratory for discussions, Prashant Jethva and Nilesh Aghera for help with MATLAB simulations, and Pooja Malhotra for help with

ETD data analysis. J.B.U is a recipient of a JC Bose National Research Fellowship from the Government of India. This work was funded by the Tata Institute of Fundamental Research and by the Department of Science and Technology, Government of India.

Appendix A. Supplementary material

Supplementary data to this article can be found online at <https://doi.org/10.1016/j.jmb.2021.167268>.

Received 25 June 2021;

Accepted 16 September 2021;

Available online 23 September 2021

Keywords:

monellin;
non-cooperative and cooperative;
kinetics;
free energy of unfolding;
entropy

Abbreviations used:

DcMN, double chain monellin; MNEI, single chain monellin; HX-MS, hydrogen exchange coupled to mass spectrometry; GdnHCl, guanidine hydrochloride; BEX, back-exchange; FWHM, full width at half maximum; ETD, electron transfer dissociation

References

- Jackson, S.E., Fersht, A.R., (1991). Folding of chymotrypsin inhibitor 2. 1. Evidence for a two-state transition. *Biochemistry*, **30**, 10428–10435.
- Yi, Q., Baker, D., (1996). Direct evidence for a two-state protein unfolding transition from hydrogen-deuterium exchange, mass spectrometry, and NMR. *Protein Sci.*, **5**, 1060–1066.
- Jackson, S.E., (1998). How do small single-domain proteins fold? *Fold Des.*, **3**, R81–R91.
- Canet, D., Last, A.M., Tito, P., Sunde, M., Spencer, A., Archer, D.B., et al., (2002). Local cooperativity in the unfolding of an amyloidogenic variant of human lysozyme. *Nature Struct. Biol.*, **9**, 308–315.
- Miranker, A., Robinson, C.V., Radford, S.E., Aplin, R.T., Dobson, C.M., (1993). Detection of transient protein folding populations by mass spectrometry. *Science*, **262**, 896–900.
- Bai, Y., Sosnick, T.R., Mayne, L., Englander, S.W., (1995). Protein folding intermediates: native-state hydrogen exchange. *Science*, **269**, 192–197.
- Englander, S.W., (2000). Protein folding intermediates and pathways studied by hydrogen exchange. *Annu. Rev. Biophys. Biomol. Struct.*, **29**, 213–238.
- Bollen, Y.J., Kamphuis, M.B., van Mierlo, C.P., (2006). The folding energy landscape of apoflavodoxin is rugged: Hydrogen exchange reveals nonproductive misfolded intermediates. *Proc. Natl. Acad. Sci.*, **103**, 4095–4100.
- Wani, A.H., Udgaonkar, J.B., (2009). Native state dynamics drive the unfolding of the SH3 domain of PI3 kinase at high denaturant concentration. *Proc. Natl. Acad. Sci.*, **106**, 20711–20716.

10. Malhotra, P., Udgaonkar, J.B., (2015). Tuning cooperativity on the free energy landscape of protein folding. *Biochemistry*, **54**, 3431–3441.
11. Jha, S.K., Udgaonkar, J.B., (2007). Exploring the cooperativity of the fast folding reaction of a small protein using pulsed thiol labeling and mass spectrometry. *J. Biol. Chem.*, **282**, 37479–37491.
12. Malhotra, P., Udgaonkar, J.B., (2014). High-energy intermediates in protein unfolding characterized by thiol labeling under natively-like conditions. *Biochemistry*, **53**, 3608–3620.
13. Udgaonkar, J.B., Baldwin, R.L., (1990). Early folding intermediate of ribonuclease A. *Proc. Natl. Acad. Sci.*, **87**, 8197–8201.
14. Krantz, B.A., Sosnick, T.R., (2000). Distinguishing between two-state and three-state models for ubiquitin folding. *Biochemistry*, **39**, 11696–11701.
15. Konermann, L., Simmons, D.A., (2003). Protein-folding kinetics and mechanisms studied by pulse-labeling and mass spectrometry. *Mass Spectrom. Rev.*, **22**, 1–26.
16. Hu, W., Walters, B.T., Kan, Z.-Y., Mayne, L., Rosen, L.E., Marqusee, S., et al., (2013). Stepwise protein folding at near amino acid resolution by hydrogen exchange and mass spectrometry. *Proc. Natl. Acad. Sci.*, **110**, 7684–7689.
17. Walters, B.T., Mayne, L., Hinshaw, J.R., Sosnick, T.R., Englander, S.W., (2013). Folding of a large protein at high structural resolution. *Proc. Natl. Acad. Sci.*, **110**, 18898–18903.
18. Sridevi, K., Lakshmikanth, G., Krishnamoorthy, G., Udgaonkar, J.B., (2004). Increasing stability reduces conformational heterogeneity in a protein folding intermediate ensemble. *J. Mol. Biol.*, **337**, 699–711.
19. Kishore, M., Krishnamoorthy, G., Udgaonkar, J.B., (2013). Critical evaluation of the two-state model describing the equilibrium unfolding of the PI3K SH3 domain by time-resolved fluorescence resonance energy transfer. *Biochemistry*, **52**, 9482–9496.
20. Halloran, K.T., Wang, Y., Arora, K., Chakravarthy, S., Irving, T.C., Bilsel, O., et al., (2019). Frustration and folding of a TIM barrel protein. *Proc. Natl. Acad. Sci.*, **116**, 16378–16383.
21. Kuzmenkina, E.V., Heyes, C.D., Nienhaus, G.U., (2006). Single-molecule FRET study of denaturant induced unfolding of RNase H. *J. Mol. Biol.*, **357**, 313–324.
22. Arrington, C.B., Teesch, L.M., Robertson, A.D., (1999). Defining protein ensembles with native-state NH exchange: kinetics of interconversion and cooperative units from combined NMR and MS analysis. *J. Mol. Biol.*, **285**, 1265–1275.
23. Malhotra, P., Udgaonkar, J.B., (2016). Secondary structural change can occur diffusely and not modularly during protein folding and unfolding reactions. *J. Am. Chem. Soc.*, **138**, 5866–5878.
24. Lakshmikanth, G., Sridevi, K., Krishnamoorthy, G., Udgaonkar, J.B., (2001). Structure is lost incrementally during the unfolding of barstar. *Nature Struct. Biol.*, **8**, 799–804.
25. Rami, B.R., Udgaonkar, J.B., (2002). Mechanism of formation of a productive molten globule form of barstar. *Biochemistry*, **41**, 1710–1716.
26. Rami, B.R., Krishnamoorthy, G., Udgaonkar, J.B., (2003). Dynamics of the core tryptophan during the formation of a productive molten globule intermediate of barstar. *Biochemistry*, **42**, 7986–8000.
27. Patra, A.K., Udgaonkar, J.B., (2007). Characterization of the folding and unfolding reactions of single-chain monellin: Evidence for multiple intermediates and competing pathways. *Biochemistry*, **46**, 11727–11743.
28. Jha, S.K., Dhar, D., Krishnamoorthy, G., Udgaonkar, J.B., (2009). Continuous dissolution of structure during the unfolding of a small protein. *Proc. Natl. Acad. Sci.*, **106**, 11113–11118.
29. McCammon, J.A., Gelin, B.R., Karplus, M., (1977). Dynamics of folded proteins. *Nature*, **267**, 585–590.
30. Bryngelson, J.D., Onuchic, J.N., Socci, N.D., Wolynes, P. G., (1995). Funnels, pathways, and the energy landscape of protein folding: a synthesis. *Proteins Struct. Funct. Bioinf.*, **21**, 167–195.
31. Henzler-Wildman, K., Kern, D., (2007). Dynamic personalities of proteins. *Nature*, **450**, 964–972.
32. Jha, S.K., Udgaonkar, J.B., (2009). Direct evidence for a dry molten globule intermediate during the unfolding of a small protein. *Proc. Natl. Acad. Sci.*, **106**, 12289–12294.
33. Kim, S.-H., de Vos, A., Ogata, C., (1988). Crystal structures of two intensely sweet proteins. *Trends Biochem. Sci.*, **13**, 13–15.
34. Aghera, N., Earanna, N., Udgaonkar, J.B., (2011). Equilibrium unfolding studies of monellin: The double-chain variant appears to be more stable than the single-chain variant. *Biochemistry*, **50**, 2434–2444.
35. Bhatia, S., Krishnamoorthy, G., Udgaonkar, J.B., (2018). Site-specific time-resolved FRET reveals local variations in the unfolding mechanism in an apparently two-state protein unfolding transition. *PCCP*, **20**, 3216–3232.
36. Bhatia, S., Krishnamoorthy, G., Dhar, D., Udgaonkar, J.B., (2019). Observation of continuous contraction and a metastable misfolded state during the collapse and folding of a small protein. *J. Mol. Biol.*, **431**, 3814–3826.
37. Bhatia, S., Krishnamoorthy, G., Udgaonkar, J.B., (2021). Mapping distinct sequences of structure formation differentiating multiple folding pathways of a small protein. *J. Am. Chem. Soc.*, **143**, 1447–1457.
38. Goluguri, R.R., Udgaonkar, J.B., (2015). Rise of the Helix from a Collapsed Globule during the Folding of Monellin. *Biochemistry*, **54**, 5356–5365.
39. Malhotra, P., Jethva, P.N., Udgaonkar, J.B., (2017). Chemical denaturants smoothen ruggedness on the free energy landscape of protein folding. *Biochemistry*, **56**, 4053–4063.
40. Jethva, P.N., Udgaonkar, J.B., (2017). Modulation of the extent of cooperative structural change during protein folding by chemical denaturant. *J. Phys. Chem. B*, **121**, 8263–8275.
41. Jethva, P.N., Udgaonkar, J.B., (2018). The osmolyte TMAO modulates protein folding cooperativity by altering global protein stability. *Biochemistry*, **57**, 5851–5863.
42. Weis, D.D., Wales, T.E., Engen, J.R., Hotchko, M., Ten Eyck, L.F., (2006). Identification and characterization of EX1 kinetics in H/D exchange mass spectrometry by peak width analysis. *J. Am. Soc. Mass Spectrom.*, **17**, 1498–1509.
43. Englander, S.W., Mayne, L., (1992). Protein folding studied using hydrogen-exchange labeling and two-dimensional NMR. *Annu. Rev. Biophys. Biomol. Struct.*, **21**, 243–265.
44. Chamberlain, A.K., Handel, T.M., Marqusee, S., (1996). Detection of rare partially folded molecules in equilibrium

- with the native conformation of RNaseH. *Nature Struct. Biol.*, **3**, 782–787.
45. Krishna, M.M., Hoang, L., Lin, Y., Englander, S.W., (2004). Hydrogen exchange methods to study protein folding. *Methods*, **34**, 51–64.
 46. Ferraro, D.M., Lazo, N.D., Robertson, A.D., (2004). EX1 hydrogen exchange and protein folding. *Biochemistry*, **43**, 587–594.
 47. Morgan, C.R., Engen, J.R., (2009). Investigating solution-phase protein structure and dynamics by hydrogen exchange mass spectrometry. *Curr. Protocols Protein Sci.*, **58** 17.6.1–6.
 48. Syka, J.E., Coon, J.J., Schroeder, M.J., Shabanowitz, J., Hunt, D.F., (2004). Peptide and protein sequence analysis by electron transfer dissociation mass spectrometry. *Proc. Natl. Acad. Sci.*, **101**, 9528–9533.
 49. Rand, K.D., Pringle, S.D., Morris, M., Engen, J.R., Brown, J.M., (2011). ETD in a traveling wave ion guide at tuned Z-spray ion source conditions allows for site-specific hydrogen/deuterium exchange measurements. *J. Am. Soc. Mass Spectrom.*, **22**
 50. Hoang, L., Bédard, S., Krishna, M.M., Lin, Y., Englander, S. W., (2002). Cytochrome c folding pathway: kinetic native-state hydrogen exchange. *Proc. Natl. Acad. Sci.*, **99**, 12173–12178.
 51. Kim, K.S., Fuchs, J.A., Woodward, C.K., (1993). Hydrogen exchange identifies native-state motional domains important in protein folding. *Biochemistry*, **32**, 9600–9608.
 52. Wales, T.E., Engen, J.R., (2006). Partial unfolding of diverse SH3 domains on a wide timescale. *J. Mol. Biol.*, **357**, 1592–1604.
 53. Fersht, A.R., (2000). A kinetically significant intermediate in the folding of barnase. *Proc. Natl. Acad. Sci.*, **97**, 14121–14126.
 54. Takei, J., Chu, R.-A., Bai, Y., (2000). Absence of stable intermediates on the folding pathway of barnase. *Proc. Natl. Acad. Sci.*, **97**, 10796–10801.
 55. Sridevi, K., Udgaonkar, J.B., (2002). Unfolding rates of barstar determined in native and low denaturant conditions indicate the presence of intermediates. *Biochemistry*, **41**, 1568–1578.
 56. Yasin, U.M., Sashi, P., Bhuyan, A.K., (2014). Free energy landscape of lysozyme: multiple near-native conformational states and rollover in the urea dependence of folding energy. *J. Phys. Chem. B*, **118**, 6662–6669.
 57. Swint-Kruse, L., Robertson, A.D., (1996). Temperature and pH dependences of hydrogen exchange and global stability for ovomucoid third domain. *Biochemistry*, **35**, 171–180.
 58. Arrington, C.B., Robertson, A.D., (1997). Microsecond protein folding kinetics from native-state hydrogen exchange. *Biochemistry*, **36**, 8686–8691.
 59. Bhuyan, A.K., Udgaonkar, J.B., (1998). Two structural subdomains of barstar detected by rapid mixing NMR measurement of amide hydrogen exchange. *Proteins Struct. Funct. Bioinf.*, **30**, 295–308.
 60. Sivaraman, T., Arrington, C.B., Robertson, A.D., (2001). Kinetics of unfolding and folding from amide hydrogen exchange in native ubiquitin. *Nature Struct. Biol.*, **8**, 331–333.
 61. Juneja, J., Udgaonkar, J.B., (2002). Characterization of the unfolding of ribonuclease A by a pulsed hydrogen exchange study: evidence for competing pathways for unfolding. *Biochemistry*, **41**, 2641–2654.
 62. Bhutani, N., Udgaonkar, J.B., (2003). Folding subdomains of thioredoxin characterized by native-state hydrogen exchange. *Protein Sci.*, **12**, 1719–1731.
 63. Moulick, R., Das, R., Udgaonkar, J.B., (2015). Partially unfolded forms of the prion protein populated under misfolding-promoting conditions: characterization by hydrogen exchange mass spectrometry and NMR. *J. Biol. Chem.*, **290**, 25227–25240.
 64. Llinás, M., Gillespie, B., Dahlquist, F.W., Marqusee, S., (1999). The energetics of T4 lysozyme reveal a hierarchy of conformations. *Nature Struct. Biol.*, **6**, 1072–1078.
 65. Hosszu, L.L., Baxter, N.J., Jackson, G.S., Power, A., Clarke, A.R., Waltho, J.P., et al., (1999). Structural mobility of the human prion protein probed by backbone hydrogen exchange. *Nature Struct. Biol.*, **6**, 740–743.
 66. Nicholson, E.M., Mo, H., Prusiner, S.B., Cohen, F.E., Marqusee, S., (2002). Differences between the prion protein and its homolog Doppel: a partially structured state with implications for scrapie formation. *J. Mol. Biol.*, **316**, 807–815.
 67. Aghera, N., Udgaonkar, J.B., (2012). Kinetic studies of the folding of heterodimeric monellin: Evidence for switching between alternative parallel pathways. *J. Mol. Biol.*, **420**, 235–250.
 68. Alexandrescu, A.T., Jaravine, V.A., Dames, S.A., Lamour, F.P., (1999). NMR hydrogen exchange of the OB-fold protein LysN as a function of denaturant: the most conserved elements of structure are the most stable to unfolding. *J. Mol. Biol.*, **289**, 1041–1054.
 69. Rodriguez, H.M., Robertson, A.D., Gregoret, L.M., (2002). Native state EX2 and EX1 hydrogen exchange of Escherichia coli CspA, a small β -sheet protein. *Biochemistry*, **41**, 2140–2148.
 70. Sugase, K., Dyson, H.J., Wright, P.E., (2007). Mechanism of coupled folding and binding of an intrinsically disordered protein. *Nature*, **447**, 1021–1025.
 71. Bachmann, A., Wildemann, D., Praetorius, F., Fischer, G., Kiefhaber, T., (2011). Mapping backbone and side-chain interactions in the transition state of a coupled protein folding and binding reaction. *Proc. Natl. Acad. Sci.*, **108**, 3952–3957.
 72. Sen, S., Udgaonkar, J.B., (2019). Binding-induced folding under unfolding conditions: Switching between induced fit and conformational selection mechanisms. *J. Biol. Chem.*, **294**, 16942–16952.
 73. Scalley-Kim, M., Baker, D., (2004). Characterization of the folding energy landscapes of computer generated proteins suggests high folding free energy barriers and cooperativity may be consequences of natural selection. *J. Mol. Biol.*, **338**, 573–583.
 74. Watters, A.L., Deka, P., Corrent, C., Callender, D., Varani, G., Sosnick, T., et al., (2007). The highly cooperative folding of small naturally occurring proteins is likely the result of natural selection. *Cell*, **128**, 613–624.
 75. Cellitti, J., Llinas, M., Echols, N., Shank, E.A., Gillespie, B., Kwon, E., et al., (2007). Exploring subdomain cooperativity in T4 lysozyme I: Structural and energetic studies of a circular permutant and protein fragment. *Protein Sci.*, **16**, 842–851.
 76. Shank, E.A., Cecconi, C., Dill, J.W., Marqusee, S., Bustamante, C., (2010). The folding cooperativity of a protein is controlled by its chain topology. *Nature*, **465**, 637–640.

77. Imamura, H., Isogai, Y., Kato, M., (2012). Differences in the structural stability and cooperativity between monomeric variants of natural and de novo Cro proteins revealed by high-pressure Fourier transform infrared spectroscopy. *Biochemistry*, **51**, 3539–3546.
78. Basak, S., Nobrega, R.P., Tavella, D., Deveau, L.M., Koga, N., Tatsumi-Koga, R., et al., (2019). Networks of electrostatic and hydrophobic interactions modulate the complex folding free energy surface of a designed $\beta\alpha$ protein. *Proc. Natl. Acad. Sci.*, **116**, 6806–6811.
79. Sakane, I., Ikeda, M., Matsumoto, C., Higurashi, T., Inoue, K., Hongo, K., et al., (2004). Structural stability of oligomeric chaperonin 10: the role of two β -strands at the N and C termini in structural stabilization. *J. Mol. Biol.*, **344**, 1123–1133.
80. Sakane, I., Hongo, K., Motojima, F., Murayama, S., Mizobata, T., Kawata, Y., (2007). Structural stability of covalently linked GroES heptamer: advantages in the formation of oligomeric structure. *J. Mol. Biol.*, **367**, 1171–1185.
81. Aghera, N., Udgaonkar, J.B., (2011). Heterologous expression, purification and characterization of heterodimeric monellin. *Protein Expr. Purif.*, **76**, 248–253.
82. Wales, T.E., Fadgen, K.E., Gerhardt, G.C., Engen, J.R., (2008). High-speed and high-resolution UPLC separation at zero degrees Celsius. *Anal. Chem.*, **80**, 6815–6820.
83. Walters, B.T., Ricciuti, A., Mayne, L., Englander, S.W., (2012). Minimizing back exchange in the hydrogen exchange-mass spectrometry experiment. *J. Am. Soc. Mass Spectrom.*, **23**, 2132–2139.